Existence of Ti^{2+} states on the surface of heavily reduced $SrTiO_3$ nanocubes

Existence of Ti^{2+} states on the surface of heavily reduced $SrTiO_3$ nanocubes

Shwetha Shetty†, Shyam Kanta Sinha‡, Rafia Ahmad†, Abhishek K Singh†, G. Van Tendeloo‡ and N. Ravishankar†*

† Materials Research Center, Indian Institute of Science, C. V. Raman Avenue, Bangalore – 560012, India

‡ EMAT, University of Antwerp, Groenenborgerlaan, 171, B-2020, Antwerpen, Belgium

KEYWORDS: $SrTiO_3$, perovskites, surfaces, reduction, oxidation state, HAADF, EELS mapping

ABSTRACT: Using advanced electron microscopy, we demonstrate the presence of Ti^{2+} on the 001 surfaces of heavily reduced strontium titanate nanocubes. While high-angle annular dark field images show a clear difference between the surfaces of the unreduced and reduced samples, electron energy loss spectroscopy detects the presence of Ti^{2+} on the surface of the reduced cubes. Conventional reduction only leads to the formation of Ti^{3+} and involves the use of high temperatures. In our case, reduction is achieved at relatively lower temperatures in the solid state using sodium borohydride as the reducing agent. Our findings provide insights into the optical properties of the samples and provide a convenient method to produce highly reduced surfaces that could demonstrate a range of exotic physical phenomena.

Oxygen vacancies in perovskite strontium titanate ($SrTiO_3$, STO) lead to fascinating properties and unique phenomena such as n-type conductivity, superconductivity, photoluminescence and visible light photocatalysis[1-6]. The presence of these vacancies also leads to the observation of a 2-dimensional electron gas (2DEG) and magnetic ordering/transient superconductivity on the bare surfaces/interfaces of STO[7-10]. At room temperature, stoichiometric STO is a transparent insulator with an indirect band gap of 3.2 eV; it has a cubic centrosymmetric structure (a= 3.905 Å) with Pm-3m symmetry where Sr ions occupy the corners of the cubic unit cell, O^{2-} ions reside at the face centers and Ti^{4+} ions are at the body centered positions. TiO_6 octahedra are corner sharing and 2 neighboring central Ti ions are bridged through an oxygen ion. An oxygen ion leaving an occupied site leaves behind a vacancy and the 2 electrons that it shares with Ti[11-13]. Extensive work done on density of states (DOS) calculations and simultaneous experimental studies have shown that when an oxygen vacancy is created, one of the electrons is localized at the Ti site making it Ti^{3+} while the other electron is in a quasi-itinerary delocalized state free for conduction[12, 14-17] However observations of oxygen-vacancy-induced metallic Ti^{2+} in STO are limited[18, 19]. Recently, it is reported that linear clustering of oxygen vacancies around the central Ti^{4+} ion can cause reduction to Ti^{2+} [20]

Heavily oxygen deficient (100) $SrTiO_{3-\delta}$ single crystals show a dramatically different optical absorption behavior as compared to pristine STO. In addition to band edge absorption, a continuous absorption of optical and IR wavelengths is observed coupled with a characteristic broad peak centered at 2.4 eV (520 nm); its intensity increases with increasing degree of reduction[4, 21-23]. This type of absorption anomaly is also seen in TiO_2 and $BaTiO_3$ under heavy reduction[24, 25]. Scanning transmission electron microscopy (STEM) accompanied with Electron Energy Loss Spectroscopy (EELS) mapping is indispensable in understanding the variations in chemical nature, valence state of cations and the arrangement of such cations at the atomic level[26]. For instance, EELS mapping carried out on heavily Ar irradiated STO single crystals, LAO/STO interface and in-situ annealed STO thin films showed a reduction in the valence state of Ti from bulk to surface[27-29]. In this study, using high resolution STEM, we show that heavily reduced 001 surface of STO nanocube shows a strikingly different atomic arrangement as compared to pure STO. EELS mapping shows the presence of Ti^{2+} states at the surface. We correlate these observations with the unusual optical properties in heavily reduced STO nanocubes. In-situ hydrogen, generated by decomposition of $NaBH_4$[30], is exploited for reducing STO nanocubes synthesized by wet-chemical method. This sample (designated as RSTO) shows a darker grey color[6] as compared to the conventionally reduced STO samples (designated as HSTO) owing to the stronger reduction condition used in the former case (Fig. 1a). Powder X-ray diffraction patterns of pure STO and reduced STO nanocubes at room temperature show virtually undistinguishable patterns (without any difference in peak broadening or shift) that can be indexed to a cubic perovskite structure with Pm-3m space group (JCPDS file # 84-0444)(Fig.S1a); calculated lattice parameter 3.908Å. Scanning electron microscopy (SEM) shows the uniformity in size and shape of the as-synthesized STO

cubes (Fig. S1b). The average size of the STO nanocube is 60 nm (Fig. S1c). Bright field and high-resolution transmission electron microscopy (BF- & HR-TEM) indicate that the cubes are predominantly bounded by {001} facets and have rounded edges (Fig. 1b & 1c). Since the synthesis methodology does not involve the use of any surfactants to control the shape of STO, the {001} surfaces are capping-free and hence well suited for studying the pristine {001} surfaces. The reduced samples show no changes in the morphology and there is no evidence for the formation of an amorphous layer on the surface of the cubes.

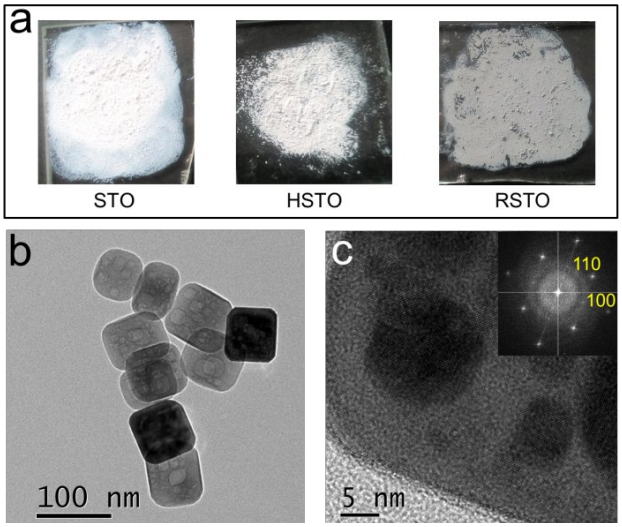

Fig.1. **(a)** Photograph of STO, HSTO and RSTO powdersamples drop-casted on glass substrates showing clear difference in color. **(b)** & **(c)** BF and HR-TEM images of as prepared STO nanocubes. Inset in **(c)** shows the Fourier transform of the high-resolution image.

Stoichiometric STO is white in color and Ti is in the 4+ valence state ($3d^0$). The conduction band in STO is mainly of Ti *3d* character, where *3d* t_{2g} states make up the bottom of the conduction band and $3de_g$ states the top, with a gap of 2.3eV between them; the valence band is mainly of O2*p* character[16]. When non-stoichiometry is introduced in the crystal in the form of oxygen vacancies, Ti can be in mixed valence state viz 4+,3+ ($3d^1$) and in the extreme cases 2+($3d^2$)[19]. When an oxygen anion leaves the crystal lattice, being an electron donor, it splits the degeneracy of the t_{2g} and e_g states of the Ti ion due to the preferential filling of the *d*-orbitals that is responsible for the color. While visual observation of the samples show clear changes in color owing to possible changes in oxidation state of Ti, X-ray photoelectron spectra (XPS) did not reveal any appreciable difference between the samples and hence could not unambiguously provide information on the changes in the oxidation state of the Ti ions (Fig S4). Hence, we relied on EELS mapping to understand the exact nature of the surface after reduction, owing to the improved spatial resolution and sensitivity to local changes that can be captured using this technique.

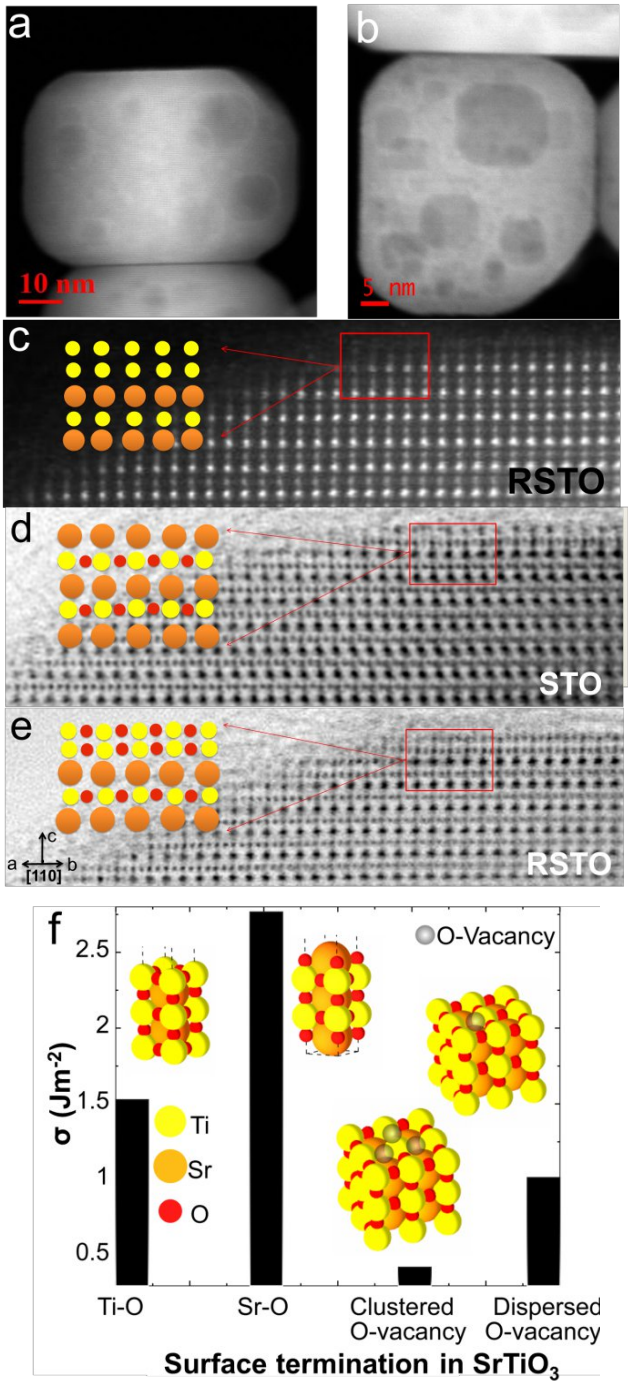

Fig.2. **(a)** & **(b)** HAADF-STEM images for STO and RSTO respectively, showing a similar morphology. **(c)** High resolution HAADF image of RSTO showing only Ti at the surface. **(d)** & **(e)** ABF-STEM image of STO and RSTO respectively. It is clear that surface arrangement of atoms is different in RSTO. The atomic arrangement in the marked region (red open box) is schematically represented towards the left of each image. **(f)** Surface formation energy calculations for Ti-O and Sr-O termination in a 001 slab of SrTiO3 and of O-vacancy dispersed and clustered around Ti in Ti-O terminated STO.

STEM observations at atomic resolutions are made on pristine as well as on reduced sample. High angle annular dark field (HAADF-STEM) images of STO and RSTO nanocubes are shown in Fig.2a & 2b. The intensity seen in HAADF images is directly proportional to Z^n, where Z is the atomic number of the elements and n varies from 1.6-2.0 depending on the collection angle of the annular dark field (ADF) detector [31-33]. The high-resolution HAADF-STEM image of the reduced nanocube (Fig.2c) shows brighter and less bright atomic columns corresponding to Sr (Z=38) and Ti (Z=22) respectively. Low atomic number elements (viz., oxygen) are hard to observe in HAADF images. Annular bright field (ABF) imaging however is sensitive to low atomic number elements[34]. The intensity of ABF images is less sensitive to the atomic number Z and proportional to $Z^{1/3}$; hence low Z elements are more easily visible in the image[35, 36]. ABF images of RSTO show a Ti-O type of reconstruction at the top 2 layers of the surface; such reconstruction is not found in pure STO nanocubes (refer Fig.2d & 2e).

To analyze the slab termination preference for 001 $SrTiO_3$, we perform first principles density functional calculations to obtain surface energies (see SI for details). To begin with, the geometrical structure is completely optimized and relaxed for Sr-O and Ti-O terminated (001) STO. The electronic band structure for the two terminations including details of atomic contributions to the bands are presented in Fig. S5. Next, to analyze the experimental observation of Ti-O terminated (001) STO, we compared the surface energies of Sr-O and Ti-O terminated (001) STO slab using the given relation,

$$\sigma = \frac{1}{2A}(E_{surf} - N_{atoms} \cdot E_{bulk})$$

where E_{surf} and E_{bulk} are the relaxed energies of the slab (respectively for both terminations) and bulk STO, respectively. N_{atoms} is the number of atoms in the supercell of the slab and A is the area of the slab considered. As shown in Fig. 2(f) the surface energies for Ti-O and Sr-O terminated STO are 1.5 and 3.09 Jm^{-2}, respectively. Therefore, the energetic preference of Ti-O termination is more as observed in the experimental results. Next objective was to study the kind of O-vacancy on this preferred structure of Ti-O terminated STO, dispersed and clustered around Ti. After performing a complete atomic structure optimization, electronic band structure was analyzed, which shows both the structures to be metallic. The in-gap states are contributed by O-vacancy (Fig. S6) Next, we determined the surface formation energies of Ti-O terminated STO with two types of oxygen vacancies. The DFT calculations reveal that the clustered vacancy structure to be substantially more stable relative to the dispersed vacancy surface by 0.53 J/m^{-2} (Fig.2f). This is consistent with recent observations (Ref 20).

To retrieve the nature of the surface of RSTO, we collected EEL spectra from the Ti $L_{3,2}$ edge (see SI for experimental details). Surface-to-interior line plots after background removal are shown in Fig. 3a for Ti-$L_{3,2}$ and for the corresponding O-*K* edge (Fig.3b). The reference spectra of Ti $L_{3,2}$ edge obtained from pure STO (Ti^{4+}) and pure TiO (Ti^{2+}) are shown in Fig. 3c. To separate the two valence states of Ti, we used the EELSMODEL program[37] for fitting the experimental spectrum using three components: i) a power-law background, ii) a reference spectrum of Ti^{2+}, and iii) a reference spectrum of Ti^{4+}. To compare the surface of STO and RSTO we obtained a line scan plot of the Ti $L_{3,2}$ and O-*K* edge starting from the surface to the interior (Fig. S7). In pure STO, the Ti-*L* line shows four characteristic peaks due to the interaction of the spin orbit split states $2p_{3/2}$ and $2p_{1/2}$ with the crystal field split states t_{2g} and e_g confirming that Ti is in a +4 oxidation state in bulk as well as on the surface. Smoothening of this fine structure and a shift in the onset energy towards low energy losses (chemical shift) is an indication of reduction in the oxidation state of Ti due to d-band filling[38]. These changes are observed in RSTO; scanning from bulk to surface, the oxidation state changes from Ti^{4+} to Ti^{2+} which we confirmed by comparing with the reference spectra for TiO. The smoothening of the O-K edge fine structure near the surface (Fig.3b) and the shift in onset edge towards higher energy losses also confirms the reduction in Ti valence state[28]. The distribution of the Ti^{2+}/Ti^{4+} oxidation states in a single reduced nanocube is presented in the form of an EELS map (Fig.3d) that clearly shows the presence of Ti^{2+} on the surface (red color) and Ti^{4+} in the bulk of the cube (green color).

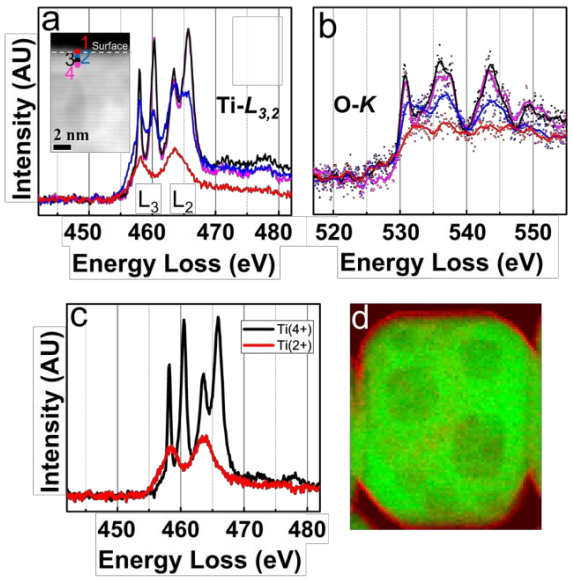

Fig.3. **(a)** & **(b)** EEL spectra obtained from regions of interest 1 to 4 are plotted for the Ti L3,2 edge and the O-K edge for RSTO. The inset in (a) is the spectrum image of RSTO and the numbers 1 to 4 represent line scan regions from surface-to-bulk **(c)** The reference spectra for Ti2+ (estimated from a standard TiO sample) and Ti4+ (from pure STO). **(d)** The output spectrum image of a RSTO nanocube after fitting. A color map of Ti2+ and Ti4+ oxidation states are marked by red and green color, respectively.

The presence of metallic Ti^{2+} causes significant changes in the optical absorption behavior of the reduced STO. UV-Vis DRS spectra and FT-IR spectra (Figs. 4a & 4b) show that RSTO absorbs over a wide range of wavelengths, all the way from the visible to the IR/MIR region (~ 10 m) whereas the unreduced sample does not show any significant absorption. The HSTO sample shows an intermediate behavior and exhibits much reduced absorption over the visible to IR range. Pure STO has band edge absorption near 400nm and is transparent to visible- NIR and MIR wavelengths. A small peak at 520 nm (2.4 eV) is seen for RSTO. In HSTO this peak is not distinctly seen. The indirect band gap value (R- transition[16]) is obtained by extrapolating the linear portion of the Tauc plot to the abscissa (Fig.S8a). An indirect band gap fits better for STO and HSTO samples and the band gap value is 3.3 eV. For RSTO the indirect band gap value obtained is 3.2 eV. However we also observed that a direct band (- transition) estimation also fits well for RSTO and the extrapolated value is 2.65 eV. A more detailed study based on density functional theory is underway to confirm this finding.

Thermal annealing studies in air are performed to check the stability of the defects introduced in RSTO (see SI for details). Corresponding absorption spectra show that there is a successive decrease in the intensity of the 520 nm peak and the broad visible-NIR absorption along with a gradual shift in the band edge towards that of STO (Fig.S8b). The color of the powder has changed from deep grey to pale grey in the course of annealing, indicating a decrease in the number of oxygen vacancies and a change

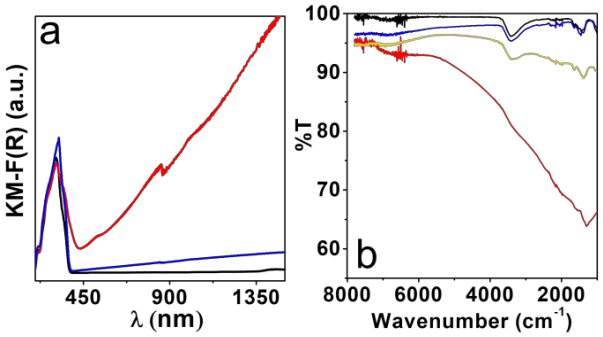

Fig.4. The curves for STO, HSTO and RSTO are represented in black, blue and red color respectively. **(a)** UV-Vis-NIR absorbance spectra (calculated from Kubelka Munk formula) for STO, HSTO and RSTO. **(b)** FT-IR spectra for STO, HSTO, RSTO and air annealed RSTO (400C-30min, yellow)

in the oxidation state of Ti. The observed optical phenomena are well studied in the literature for oxygen-deficient single crystals of STO[21, 22, 39-41]. MIR absorption is also seen in heavily reduced $BaTiO_3$[42]. Calvani et.al. observed that the intensity of the MIR absorption increases with the degree of reduction (or increase in the number of free carrier density)[22]. We have seen a similar trend for the air-annealed sample (400°C-30min) and for HSTO (Fig.4b). MIR absorption is considerably less for these samples than for RSTO. The secondary features in the FTIR spectra are discussed in detail in the supporting information. Photoluminescence studies indicate that STO and RSTO have drastically different PL properties. STO nanocubes are luminescent upon excitation whereas in RSTO, quenching of this PL band is seen (Fig.S10). STO shows a broad PL peak having a tail at the higher wavelengths indicating that several types of recombination processes are governing it (see inset of Fig S10) while in RSTO, PL is completely quenched. Nanoparticles of STO show PL at room temperature due to size confinement, structural inhomogeneity at the surface, atomic vacancies or impurities[43-45]. In RSTO we have introduced a large number of oxygen vacancies and this in turn doped the STO with a high density of free carriers. A combination of luminescence quenching processes like plasma screening and non-radiative Auger recombination [46-50] could be the reason for such luminescence quenching.

In summary, we conclude that a significant amount of oxygen vacancies can be created on the surface of STO by solid-state $NaBH_4$ reduction and the vacancy concentration can be tuned by annealing at different temperatures. Such reduced STO shows an anomalous optical absorption behavior in the visible, IR and MIR region. A small peak is seen at 2.4 eV whose intensity increases with the degree of reduction. IR studies also reveal the possibility of having different surface chemistry for pure and reduced surfaces. STEM studies reveal a surface reconstruction in heavily reduced STO samples and EELS mapping shows Ti^{2+} in the first 2 monolayers from the surface. Optical absorption anomalies and PL quenching can be correlated to the above findings.

AUTHOR INFORMATION

Corresponding Author

* N. Ravishankar. Email: nravi@mrc.iisc.ernet.in

Author Contributions

The manuscript was written through contributions of all authors. All authors have given approval to the final version of the manuscript.

Funding Sources

SS and NR acknowledge Department of Science and Technology (DST), India for the funding under DST-Nanomission scheme.

Notes

The authors declare no competing financial interest.

ACKNOWLEDGMENT

We thank Advanced Facility for Microscopy and Microanalysis (AFMM), IISc, Bangalore for providing the TEM facility. We also thank MNCF, CeNSE, IISc for providing the XPS and FT-IR facilities. We acknowledge the help from Prof. Anshu Pandey for providing the PL facility and Mr. Ashutosh Gupta for the help with measurements. SS and NR thank DST for providing the financial support.

RA and AKS acknowledge Super Computing Education and Research Center (SERC) and Materials Research Center (MRC), at IISc for providing required computational facilities. RA acknowledges the financial support from INSPIRE fellowship, AORC.

REFERENCES

1. Schooley, J.; Hosler, W.; Cohen, M. L., Superconductivity in Semiconducting SrTi O 3. *Physical Review Letters* **1964,** 12, (17), 474.
2. Balachandran, U.; Eror, N., Electrical conductivity in strontium titanate. *Journal of Solid State Chemistry* **1981,** 39, (3), 351-359.
3. Koonce, C.; Cohen, M. L.; Schooley, J.; Hosler, W.; Pfeiffer, E., Superconducting Transition Temperatures of Semiconducting SrTi O 3. *Physical Review* **1967,** 163, (2), 380.
4. Rice, W.; Ambwani, P.; Bombeck, M.; Thompson, J.; Haugstad, G.; Leighton, C.; Crooker, S., Persistent optically induced magnetism in oxygen-deficient strontium titanate. *Nature materials* **2014,** 13, (5), 481-487.
5. Xu, W.; Yang, J.; Bai, W.; Tang, K.; Zhang, Y.; Tang, X., Oxygen vacancy induced photoluminescence and ferromagnetism in SrTiO3 thin films by molecular beam epitaxy. *Journal of Applied Physics* **2013,** 114, (15), 154106.
6. Tan, H.; Zhao, Z.; Zhu, W.-b.; Coker, E. N.; Li, B.; Zheng, M.; Yu, W.; Fan, H.; Sun, Z., Oxygen vacancy enhanced photocatalytic activity of pervoskite SrTiO3. *ACS applied materials & interfaces* **2014,** 6, (21), 19184-19190.
7. Santander-Syro, A.; Copie, O.; Kondo, T.; Fortuna, F.; Pailhes, S.; Weht, R.; Qiu, X.; Bertran, F.; Nicolaou, A.; Taleb-Ibrahimi, A., Two-dimensional electron gas with universal subbands at the surface of SrTiO3. *Nature* **2011,** 469, (7329), 189-193.
8. Ohtomo, A.; Hwang, H., A high-mobility electron gas at the LaAlO3/SrTiO3 heterointerface. *Nature* **2004,** 427, (6973), 423-426.
9. Brinkman, A.; Huijben, M.; Van Zalk, M.; Huijben, J.; Zeitler, U.; Maan, J.; Van der Wiel, W.; Rijnders, G.; Blank, D.; Hilgenkamp, H., Magnetic effects at the interface between non-magnetic oxides. *Nature materials* **2007,** 6, (7), 493-496.
10. Daptary, G. N.; Kumar, S.; Bid, A.; Kumar, P.; Dogra, A.; Budhani, R.; Kumar, D.; Mohanta, N.; Taraphder, A., Observation of transient superconductivity at the LaAlO 3/SrTiO 3 interface. *Physical Review B* **2017,** 95, (17), 174502.
11. Cai, H.; Wu, X.; Gao, J., Effect of oxygen content on structural and transport properties in SrTiO 3− x thin films. *Chemical Physics Letters* **2009,** 467, (4), 313-317.
12. Dudy, L.; Sing, M.; Scheiderer, P.; Denlinger, J. D.; Schütz, P.; Gabel, J.; Buchwald, M.; Schlueter, C.; Lee, T. L.; Claessen, R., In Situ Control of Separate Electronic Phases on SrTiO3 Surfaces by Oxygen Dosing. *Advanced Materials* **2016,** 28, (34), 7443-7449.
13. Li, W.; Liu, S.; Wang, S.; Guo, Q.; Guo, J., The Roles of Reduced Ti Cations and Oxygen Vacancies in Water Adsorption and Dissociation on SrTiO3 (110). *The Journal of Physical Chemistry C* **2014,** 118, (5), 2469-2474.
14. Jeschke, H. O.; Shen, J.; Valentí, R., Localized versus itinerant states created by multiple oxygen vacancies in SrTiO3. *New Journal of Physics* **2015,** 17, (2), 023034.
15. Lin, C.; Demkov, A. A., Electron correlation in oxygen vacancy in SrTiO 3. *Physical review letters* **2013,** 111, (21), 217601.
16. Luo, W.; Duan, W.; Louie, S. G.; Cohen, M. L., Structural and electronic properties of n-doped and p-doped Sr Ti O 3. *Physical Review B* **2004,** 70, (21), 214109.
17. Shanthi, N.; Sarma, D., Electronic structure of electron doped SrTiO 3: SrTiO 3− δ and Sr 1− x La x TiO 3. *Physical Review B* **1998,** 57, (4), 2153.
18. Lee, S. B.; Phillipp, F.; Sigle, W.; Rühle, M., Nanoscale TiO island formation on the SrTiO 3 (001) surface studied by in situ high-resolution transmission electron microscopy. *Ultramicroscopy* **2005,** 104, (1), 30-38.
19. Marshall, M. S.; Becerra-Toledo, A. E.; Marks, L. D.; Castell, M. R., Surface and defect structure of oxide nanowires on SrTiO 3. *Physical review letters* **2011,** 107, (8), 086102.
20. Eom, K.; Choi, E.; Choi, M.; Han, S.; Zhou, H.; Lee, J., Oxygen Vacancy Linear Clustering in a Perovskite Oxide. *The Journal of Physical Chemistry Letters* **2017,** 8, (15), 3500-3505.
21. Yamada, H.; Miller, G., Point defects in reduced strontium titanate. *Journal of Solid State Chemistry* **1973,** 6, (1), 169-177.
22. Calvani, P.; Capizzi, M.; Donato, F.; Lupi, S.; Maselli, P.; Peschiaroli, D., Observation of a midinfrared band in SrTiO 3− y. *Physical Review B* **1993,** 47, (14), 8917.
23. Wild, R.; Rockar, E. M.; Smith, J. C., Thermochromism and Electrical Conductivity in Doped SrTi O 3. *Physical Review B* **1973,** 8, (8), 3828.
24. Chiesa, M.; Livraghi, S.; Giamello, E.; Albanese, E.; Pacchioni, G., Ferromagnetic Interactions in Highly Stable, Partially Reduced TiO2: The S= 2 State in Anatase. *Angewandte Chemie International Edition* **2017,** 56, (10), 2604-2607.
25. Schrader, M.; Mienert, D.; Oh, T.-S.; Yoo, H.-I.; Becker, K. D., An optical, EPR and electrical conductivity study of blue barium titanate, BaTiO 3− δ. *Solid State Sciences* **2008,** 10, (6), 768-775.
26. Goris, B.; Turner, S.; Bals, S.; Van Tendeloo, G., Three-dimensional valency mapping in ceria nanocrystals. *ACS nano* **2014,** 8, (10), 10878-10884.
27. Muller, D. A.; Nakagawa, N.; Ohtomo, A.; Grazul, J. L.; Hwang, H. Y., Atomic-scale imaging of nanoengineered oxygen vacancy profiles in SrTiO3. *Nature* **2004,** 430, (7000), 657-661.
28. Sánchez-Santolino, G.; Tornos, J.; Bruno, F. Y.; Cuellar, F.; Leon, C.; Santamaría, J.; Pennycook, S.; Varela, M., Characterization of surface metallic states in SrTiO 3 by means of aberration corrected electron microscopy. *Ultramicroscopy* **2013,** 127, 109-113.
29. Xu, W.; Bowes, P. C.; Grimley, E. D.; Irving, D. L.; LeBeau, J. M., In-situ real-space imaging of single crystal surface reconstructions via electron microscopy. *Applied Physics Letters* **2016,** 109, (20), 201601.
30. Martelli, P.; Caputo, R.; Remhof, A.; Mauron, P.; Borgschulte, A.; Züttel, A., Stability and decomposition of NaBH□. *The Journal of Physical Chemistry C* **2010,** 114, (15), 7173-7177.
31. Jesson, D.; Pennycook, S. In *Incoherent imaging of crystals using thermally scattered electrons*, Proceedings of the Royal Society of London A: Mathematical, Physical and Engineering Sciences, 1995; The Royal Society: 1995; pp 273-293.
32. Wang, Z.; Li, Z.; Park, S.; Abdela, A.; Tang, D.; Palmer, R., Quantitative Z-contrast imaging in the scanning transmission electron microscope with size-selected clusters. *Physical Review B* **2011,** 84, (7), 073408.
33. Hartel, P.; Rose, H.; Dinges, C., Conditions and reasons for incoherent imaging in STEM. *Ultramicroscopy* **1996,** 63, (2), 93-114.
34. Ishikawa, R.; Okunishi, E.; Sawada, H.; Kondo, Y.; Hosokawa, F.; Abe, E., Direct imaging of hydrogen-atom columns in a crystal by annular bright-field electron microscopy. *Nature materials* **2011,** 10, (4), 278.
35. Okunishi, E.; Ishikawa, I.; Sawada, H.; Hosokawa, F.; Hori, M.; Kondo, Y., Visualization of light elements at ultrahigh resolution by STEM annular bright field microscopy. *Microscopy and Microanalysis* **2009,** 15, (S2), 164.
36. Findlay, S.; Shibata, N.; Sawada, H.; Okunishi, E.; Kondo, Y.; Ikuhara, Y., Dynamics of annular bright field imaging in scanning transmission electron microscopy. *Ultramicroscopy* **2010,** 110, (7), 903-923.
37. Verbeeck, J.; Van Aert, S., Model based quantification of EELS spectra. *Ultramicroscopy* **2004,** 101, (2), 207-224.
38. Stoyanov, E.; Langenhorst, F.; Steinle-Neumann, G., The effect of valence state and site geometry on Ti L3, 2 and OK electron energy-loss spectra of TixOy phases. *American Mineralogist* **2007,** 92, (4), 577-586.

39. Cohen, M.; Casella, R.; Blunt, R.; Forman, R., Lattice absorption in strontium titanate. *Physical Review* **1969,** 186, (3), 834.
40. Crandles, D.; Nicholas, B.; Dreher, C.; Homes, C.; McConnell, A.; Clayman, B.; Gong, W.; Greedan, J., Optical properties of highly reduced SrTiO 3− x. *Physical Review B* **1999,** 59, (20), 12842.
41. Van Mechelen, J.; Van der Marel, D.; Grimaldi, C.; Kuzmenko, A.; Armitage, N.; Reyren, N.; Hagemann, H.; Mazin, I., Electron-phonon interaction and charge carrier mass enhancement in SrTiO 3. *Physical review letters* **2008,** 100, (22), 226403.
42. Hwang, J.; Kolodiazhnyi, T.; Yang, J.; Couillard, M., Doping and temperature-dependent optical properties of oxygen-reduced BaTiO 3− δ. *Physical Review B* **2010,** 82, (21), 214109.
43. Mochizuki, S.; Fujishiro, F., Optical and dielectric studies on nanoparticles and atomically□engineered surfaces of superparaelectric SrTiO3. *physica status solidi (c)* **2007,** 4, (2), 515-517.
44. Souza, A.; Santos, G.; Barra, B.; Macedo Jr, W.; Teixeira, S.; Santos, C.; Senos, A.; Amaral, L.; Longo, E., Photoluminescence of SrTiO3: influence of particle size and morphology. *Crystal Growth & Design* **2012,** 12, (11), 5671-5679.
45. Zhang, W.; Yin, Z.; Zhang, M., Study of photoluminescence and electronic states in nanophase strontium titanate. *Applied Physics A* **2000,** 70, (1), 93-96.
46. Yasuda, H.; Kanemitsu, Y., Dynamics of nonlinear blue photoluminescence and Auger recombination in SrTiO 3. *Physical Review B* **2008,** 77, (19), 193202.
47. Gordon, N.; Allen, J., Auger quenching of luminescence in ZnS: Mn. *Solid State Communications* **1981,** 37, (5), 441-443.
48. Sinha, K.; DiDomenico Jr, M., Effects of plasma screening and Auger recombination on the luminescent efficiency in GaP. *Physical Review B* **1970,** 1, (6), 2623.
49. Suchocki, A.; Langer, J. M., Auger effect in the Mn 2+ luminescence of CdF 2:(Mn, Y) crystals. *Physical Review B* **1989,** 39, (11), 7905.
50. Wang, F.; Dukovic, G.; Knoesel, E.; Brus, L. E.; Heinz, T. F., Observation of rapid Auger recombination in optically excited semiconducting carbon nanotubes. *Physical Review B* **2004,** 70, (24), 241403.

Insert Table of Contents artwork here

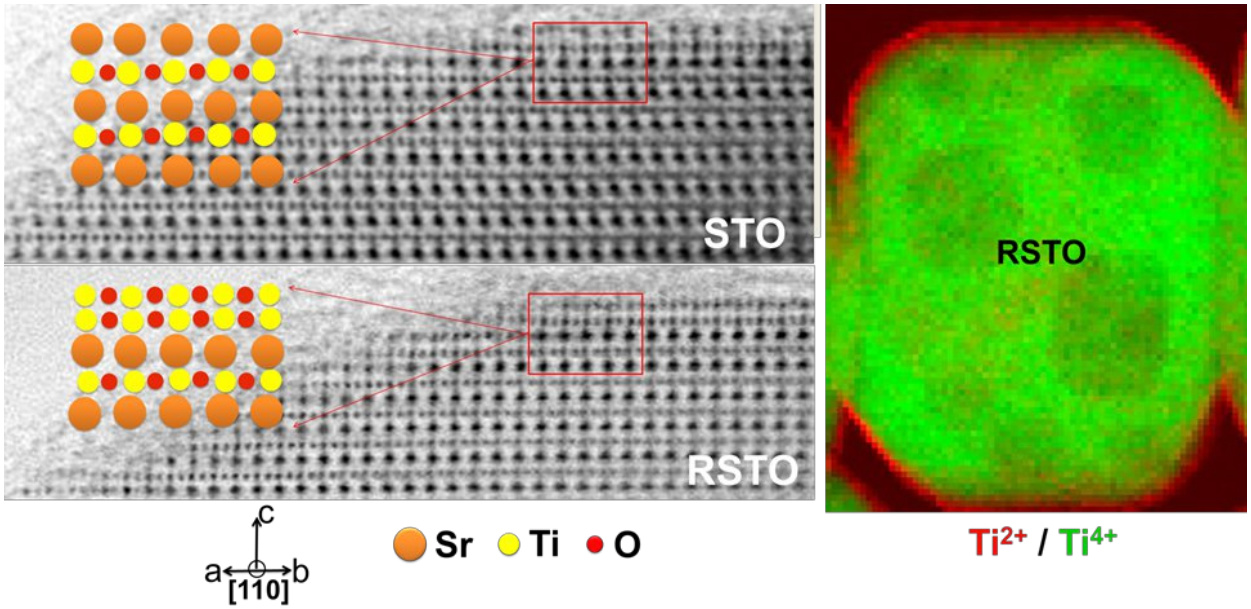
STO
RSTO
RSTO
c
a
b
[110]
Sr
Ti
O
Ti2+ / Ti4+